How to cite: *Angew. Chem. Int. Ed.* **2022,** *61,* e202117698
International Edition: doi.org/10.1002/anie.202117698
German Edition: doi.org/10.1002/ange.202117698

Zeolite Synthesis

Realizing Fast Synthesis of High-Silica Zeolite Y with Remarkable Catalytic Performance

Dali Zhu, Linying Wang, Wenna Zhang, Dong Fan, Jinzhe Li, Wenhao Cui, Shengjun Huang, Shutao Xu, Peng Tian, and Zhongmin Liu**

Abstract: High-silica zeolite Y (FAU) plays a vital role in (petro)chemical industries. However, the slow nucleation and growth kinetics of the high-silica FAU framework limit its direct synthesis and the improvement of framework SiO_2/Al_2O_3 ratio (SAR). Here, a facile strategy is developed to realize the fast crystallization of high-silica zeolite Y, which involves the combination of high crystallization temperature, ultra-stable Y (USY) seeds and efficient organic-structure directing agent (OSDA). The synthesis can be finished in 5–16 h at 160 °C and with tunable SAR up to 18.2, and the key factors affecting crystallization kinetics and phase purity are elucidated. Moreover, the crystallization process was monitored to reveal the fast crystal growth mechanism. The high-silica products possess high (hydro)thermal stability and abundant strong acid sites, which endow them excellent catalytic cracking performance, obviously superior to commercial USY.

Introduction

Zeolites are inorganic crystalline aluminosilicates with uniform pores of molecular dimension, which have found widely industrial applications in adsorption, separation and heterogeneous catalysis.[1] Zeolite Y (FAU), which has a 3D 12-membered ring channel system and spherical nanosized cavities, represents one of the most important members in zeolite family. The application of zeolite Y as the catalysts for the fluid catalytic cracking (FCC) and hydrocracking processes has been regarded as a milestone in oil refining industry, which revolutionized the processes with significantly enhanced gasoline yield and efficient utilization of petroleum feedstocks.[2] Nowadays, zeolite Y also behaves great potential in processing renewable resources.[3]

High framework SiO_2/Al_2O_3 ratio (SAR) has been demonstrated to be the decisive factor for zeolite Y to possess strong acidity and good (hydro)thermal stability, both of which are essential for its catalytic application.[4] Over the past decades, great efforts have been devoted to improving the SAR of zeolite Y. Post-synthesis dealumination, routinely performed by steaming/acid leaching to remove Al atoms from the framework is the common method for the preparation of high-silica Y.[5] Nevertheless, the loss of crystallinity and mass as well as the creation of dealumination gradient is always inevitable for the post-treatment processes.[6] Direct synthesis of high-silica Y is undoubtedly the most attractive way. Typically, the SAR of zeolite Y from inorganic system is less than 6.5,[7] which has to require a subsequent dealumination to enhance the framework SAR in order to satisfy the requirements of industrial application. Utilizing organic structure-directing agents (OSDAs) could help improve framework SAR, which has worked effectively for widening the compositions of zeolitic materials.[8] However, even with the assistance of OSDA, the SAR of zeolite Y has long been limited to 9.0, which was achieved by using crown ether as OSDA after crystallization for 8 days.[9] Recently, we developed a NOA-co strategy for the synthesis of zeolite Y.[10] A series of quaternary alkylammonium ions are discovered to be effective OSDA, and the product can reach a SAR of 15.6 with tetrabutylammonium hydroxide (TBAOH) and tetraethylammonium hydroxide (TEAOH) as co-OSDAs (crystallization for 6.5 days, 37.8 % yield). The solid yields showed a decreasing trend following the increase of product SAR. During our manuscript preparation, Dusselier et al. reported the synthesis of high-silica Y with SAR up to 12.8 (crystallization for 5 days, ≈38 % yield) by using 15-crown-5 and choline ion as co-OSDAs.[11]

Besides the improvement of framework SAR, another long-standing challenge for the synthesis of zeolite Y is how to break the kinetic limitations on the growth of high-silica framework. Significantly prolonged time is generally required for a well-crystallized product with slightly improved

[*] D. Zhu, Dr. L. Wang, Dr. W. Zhang, Dr. D. Fan, Prof. J. Li, W. Cui, Prof. S. Xu, Prof. P. Tian, Prof. Z. Liu
National Engineering Laboratory for Methanol to Olefins,
Dalian National Laboratory for Clean Energy,
Dalian Institute of Chemical Physics,
Chinese Academy of Sciences
Dalian 116023 (P. R. China)
E-mail: tianpeng@dicp.ac.cn
liuzm@dicp.ac.cn
D. Zhu, W. Cui
University of Chinese Academy of Sciences
Beijing 100049 (P. R. China)
Prof. S. Huang
Division of Fossil Energy Conversion,
Dalian National Laboratory for Clean Energy,
Dalian Institute of Chemical Physics,
Chinese Academy of Sciences
Dalian 116023 (P. R. China)

SAR.[9,10,12] Moreover, the high-silica products tend to be contaminated by amorphous materials or impurities when attempting to enhance the framework SAR. This is due to the high energy barriers for nucleation and crystal growth under the lowered alkalinity employed for the synthesis of high-silica Y.[13] Enhancing temperature is a direct way to fasten the crystallization kinetics.[14] Unfortunately, the crystallization temperature of zeolite Y hitherto cannot exceed 130 °C.[11,15] Further increasing the temperature always causes phase transformation and impurities.[16] Thus, to develop effective strategy to realize the synchronous improvement of framework SAR and crystallization kinetics would be highly desirable both for fundamental studies and industrial applications.

Herein, we report for the first time the fast synthesis of zeolite Y with unprecedentedly high SAR of 18.2 by a rationally developed strategy, which involves high crystallization temperature, USY zeolite seeds and efficient OSDA (TBAOH). The induction activity of the seeds with different SARs is investigated and revealed to be determined by the properties of their etched fragments in the starting synthetic gel. Theoretical calculations further demonstrate that compared with other OSDAs, TBAOH has strong stabilization effect for the FAU framework at elevated temperature and thus allows successful synthesis. Moreover, the fast synthesis of high-silica zeolite Y is successfully scaled up with a 10 L autoclave and the resulting material exhibits superior catalytic cracking performances.

Results and Discussion

The fast synthesis of high-silica zeolite Y (named FSY) was carried out from a gel with molar composition of $1\,SiO_2:1/x\,Al_2O_3:y\,NaOH:0.4\,TBAOH:20\,H_2O$ ($x=38$–67) at 160 °C with the addition of high-silica USY as seeds. Table 1 presents the detailed synthetic parameters and the corresponding results. From Table 1, well-crystallized high-silica zeolite Y (sample FSY-$5h_{11.8}$) can be achieved after crystallization at 160 °C for 5 hours with a gel SAR of 38 and gel alkalinity of $OH^-/Si=0.60$. Lowering the gel alkalinity to 0.52 can significantly enhance the product SAR to 16.0 (sample FSY-$16h_{16.0}$) together with an increased solid yield (from 30 % to 42 %). Meanwhile, the time for complete crystallization needs to be prolonged from 5 h to 16 h, which should result from the incremental energy barrier under lower alkalinity.[16] Increasing the initial gel SAR to 57, the product SAR displays a corresponding increase, as compared with that of gel system of SAR = 38. The FSY zeolite with the highest SAR of 18.2 (sample FSY-$16h_{18.2}$) can be achieved after 16 hours from a system from low gel alkalinity of $OH^-/Si=0.50$. Attempting to further reduce the gel alkalinity ($OH^-/Si=0.48$) or increase the gel SAR (SAR = 67), unfortunately, would give rise to products with impurity (MEL zeolite). The above results demonstrate that the present synthetic strategy can achieve unprecedentedly high SAR together with fast crystallization rate for high-silica zeolite Y, both of which have long been considered as challenging goals.

Figure 1a shows the powder X-ray diffraction (XRD) diffraction patterns of samples FSY-$5h_{13.8}$ and FSY-$16h_{18.2}$, which exhibit the typical diffraction peaks of FAU structure. The N_2 adsorption isotherms of the samples are given in Figure 1b, which present a type I isotherm. The micropore volumes of FSY-$5h_{13.8}$ and FSY-$16h_{18.2}$ are 0.30 and 0.29 $cm^3\,g^{-1}$, respectively, a bit higher than that of reference NaY_{ref} zeolite (Table S1), evidencing the high crystallinity of the synthesized high-silica materials. The phase purity of the samples is further confirmed by scanning electron microscopy (SEM) images (Figure 1c and d), showing aggregated intergrowth morphology with inhomogeneous crystal sizes. This is a common phenomenon for the seeds-assisted crystallization due to secondary nucleation.[17] The local Si atomic environments of the as-made samples were investigated by solid-state ^{29}Si MAS NMR (Figure 1e and f), showing the existence of four Si species in the framework. The strong resonances are ascribed to Si(4Si) and Si(3Si, 1Al), and the two weak ones arise from Si(2Si, 2Al) and Si(3Si)(1OH). Compared with FSY-$5h_{13.8}$, FSY-$16h_{18.2}$ clearly possesses more Si(4Si) species. Based on the deconvoluted ^{29}Si NMR spectra (Table S2), the framework SAR of FSY-$5h_{13.8}$ and FSY-$16h_{18.2}$ is calculated to be 13.8 and 18.1, respectively, in good agreement with the XRF results. Furthermore, the (hydro)thermal stability of FSY-$5h_{13.8}$ was investigated by thermal analysis and high-temperature stream treatment. From Figure S2, the results demonstrate

Table 1: Syntheses and product properties of the high-silica FSY zeolites.

Sample	x	Y	OH^-/Si	t [h]	SAR[a]	Yield [%][b]
FSY-5h11.8	38	0.20	0.60	5	11.8	30.5
FSY-16h16.0	38	0.12	0.52	16	16.0	42.2
FSY-5h13.8[c]	57	0.20	0.60	5	13.8	24.2
FSY-14h17.5	57	0.12	0.52	14	17.5	30.3
FSY-16h18.2	57	0.10	0.50	16	18.2	31.5
FSY-16hMEL	67	0.10	0.50	16	–	–
FSY-10h15.7[d]	38	0.12	0.52	10	15.7	40.8

The fast synthesis of high-silica zeolite Y (named FSY) was carried out from a gel with molar composition of $1SiO_2:1/xAl_2O_3:y\,NaOH:0.4\,TBAOH:20\,H_2O$ at 160 °C with the addition of $USY_{38.4}$ as seeds (9.5 % addition relative to SiO_2 source). The crystallization temperature is 160 °C. [a] Measured by XRF. [b] Yield was calculated based on the dry mass of SiO_2 and Al_2O_3 ($M_{product}/M_{(gel+seeds)}$ * 100 %). [c] Unit cell composition was $(H_2O)_{52.7}Na_{13.8}TBA_{10.5}(Si_{167.7}Al_{24.3}O_{384})$ calculated on the basis of TGA and XRF results. [d] $USY_{106.1}$ (in NH_4^+ form) as seeds (9.5 wt % relative to SiO_2 source).

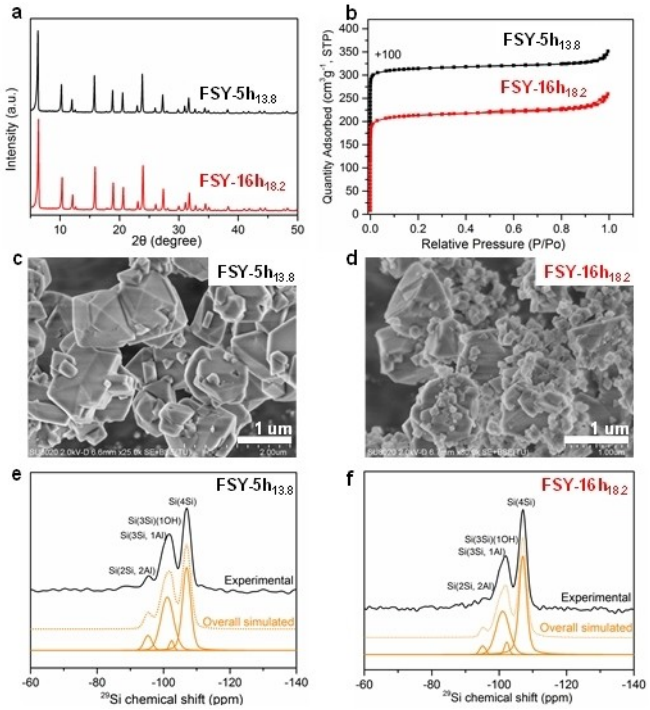

Figure 1. Physicochemical properties of high-silica FSY zeolites. a) XRD patterns, b) N_2 sorption isotherms, c), d) SEM and TEM images, d)–f) ^{29}Si MAS NMR spectra. As-made samples are used for a, c, d, e and f, whereas calcined sample for b.

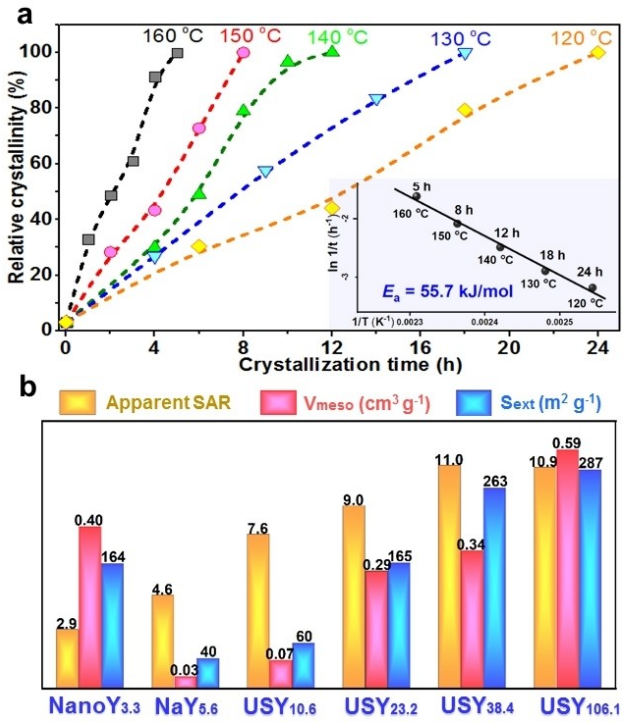

Figure 2. a) Crystallization curves at different temperatures based on the gel system of sample FSY-5h$_{13.8}$ (OH^-/Si = 0.60, USY$_{38.4}$ as seeds). b) The properties of the seeds after aging in initial synthesis gel without the addition of silica source.

that the high siliceous nature endows FSY outstanding (hydro)thermal stability, which would be of great importance for their catalytic application.

The effect of crystallization temperature on the synthesis of high-silica Y zeolite is investigated based on the gel system of FSY-5h$_{13.8}$. From Figure 2a, it is apparent that the crystallization rate of zeolite FSY increases with the temperature. Under higher temperature of 160 °C, the synthesis can be completed in 5 h. Improving the crystallization temperature to 170 °C, however, would cause the formation of MEL impurity. Interestingly, the relationship between the crystallization time and temperature are approximately in accordance with Arrhenius equation. From the slope of this curve, the apparent activation energy for the crystal growth of FSY zeolite can be estimated to be 55.7 kJ mol^{-1}. This value is comparable to those of conventional Y zeolites synthesized from inorganic systems,[13] which consists with the fast crystallization rate of FSY zeolite. It is noted that previous syntheses of zeolite Y were normally conducted at moderate temperatures (lower than 120 °C) to avoid the formation of undesired phases or transformation to more dense structures.[16] Herein, the much wide temperature range for the synthesis of FSY implies the powerful effect of the present strategy utilizing TBAOH and USY seeds on maintaining the phase purity.

To figure out the role of solid seeds, control synthesis of FSY zeolite without the addition of seeds was first performed. From Figure S3a, only amorphous product is obtained after 5 h at 160 °C. Further prolonging the time to 48 h gives rise to the appearance of MEL-type material. With a seeds addition of 5.0 wt %, the product phase, SAR and yield show high similarity to those with 9.5 wt % seeds addition, except the prolonged time for complete crystallization (Figure S3b). In addition, a series of Y zeolites with different SAR and crystallite sizes (Figure S1) were attempted as seeds for the synthesis. As displayed in Figure S4, zeolite Y in high purity can be rapidly synthesized only with the assistance of high-silica USY seeds. Compared with other seeds, the synthesis using USY$_{106.1}$ exhibits higher efficiency, which requires shorter time for complete crystallization when employing the same gel compositions (FSY-16h$_{16.0}$ vs. FSY-10h$_{15.7}$ in Table 1). Overall, the induction ability of the seeds has an order of USY$_{106.1}$ > USY$_{38.4}$ ≈ USY$_{23.2}$ > USY$_{10.6}$ > NaY$_{5.6}$ > NaY$_{nano3.3}$. However, it is noted that even with the presence of effective seeds, a gel aging process before the crystallization is necessary to realize the fast synthesis of the high-silica zeolite Y (Figure S5), implying the importance of the activation of seeds in the initial gel.

To better understand the distinct induction abilities of the seeds, their dissolution behaviors in initial synthesis gel without the addition of silica source are investigated. The detailed treatment conditions are given in the support information and the results are displayed in Figure 2b, S6 and Table S3. It is clear that the crystallinity, compositions and textural properties of the high-silica USY seeds were significantly modified upon alkaline treatment. The etched USY$_{106.1}$, USY$_{38.4}$ and USY$_{23.2}$ possess similar apparent SAR

(9–11), far lower than that of pristine seeds. The mismatch between the relatively high yields and significantly reduced SAR of the etched seeds suggests the dissolution of silica species from Si-rich seeds and the deposition of liquid-phase Al species. Importantly, the extraction of silica species from pristine seeds results in a remarkable mesoporosity development in the etched seeds (Figure S7). From Table S3 and Figure 2b, the etched high-silica USY seeds possess large external surface area (S_{exter}) and mesoporous volume (V_{meso}). In particular, the S_{exter} and V_{meso} of the etched $USY_{106.1}$ are as high as 287 m^2g^{-1} and 0.59 cm^3g^{-1}, respectively. Given that the ineffectiveness of the dissolved species for inducing crystallization (Figure S8), it is speculated that the powerful induction ability of high-silica seeds might be closely related with the large S_{exter} and V_{meso} of their etched products, which provide abundant surface for crystal growth and secondary nucleation. The $USY_{10.6}$ and $NaY_{5.6}$ show high resistance to alkaline gel according to their higher yields after treatment, which should be due to their relatively low SAR. Their S_{exter} did not exceed 60 m^2g^{-1}, unfavorable for them to act as highly active growth centers. Moreover, the etched $NaY_{nano3.3}$ shows an impressive mesoporosity and large S_{exter}, likely owing to its physique of nanocrystallites. Its failure for inducing crystal growth suggests that the composition of seeds should be also a key factor determining the inducing activity. It is thus summarized that the etching of the seeds in the aging process of the initial alkaline gel is important for the improvement of their induction ability; both higher SAR, large S_{exter} and V_{meso} are essential for the etched seeds to induce the fast crystallization of high-silica Y.

Given the importance of OSDA in the synthesis of zeolites,[18] three other OSDAs, which have been reported to be effective for the synthesis of high-silica Y at 100–120 °C, were also chosen and employed for synthesis exploration at 160 °C ($USY_{38.4}$ as seeds). They were TEAOH,[12a] tetrapropyl ammonium hydroxide (TPAOH)[10] and 1-butyl-3-methylimidazolium bromide (BMIMBr).[19] From Figure 3, the type of OSDAs greatly affects the product phase and only TBAOH can lead to the fast synthesis of high-silica Y at 160 °C. When TEAOH is employed, it delivers low crystallinity product likely arising from solid seeds after 5 h. Extending the crystallization time to 36 h, Beta is obtained as the dominant phase. With BMIMBr as OSDA, the crystallized product becomes MOR. Compared with TEAOH and BMIMBr, TPAOH shows an enhanced ability for the synthesis of high-silica zeolite Y at 160 °C, but the products contain ZSM-5 impurity. Moreover, the combination of TEAOH and TBAOH, which was employed in our previous NOA-co strategy, was also explored for the synthesis at 160 °C. Only amorphous product, however, can be obtained. These results evidence the distinct structure directing abilities of these OSDAs. Among them, TBA^+ is the most powerful one for inducing the fast crystallization of high-silica zeolite Y.

To get a clear understanding on the fast crystallization, the crystallization process of FSY-$16h_{16.0}$ (Table 1) was monitored by characterizing the solids extracted from the growth solution at periodic times (Figure 4). From the XRD patterns, no induction period can be perceived. The

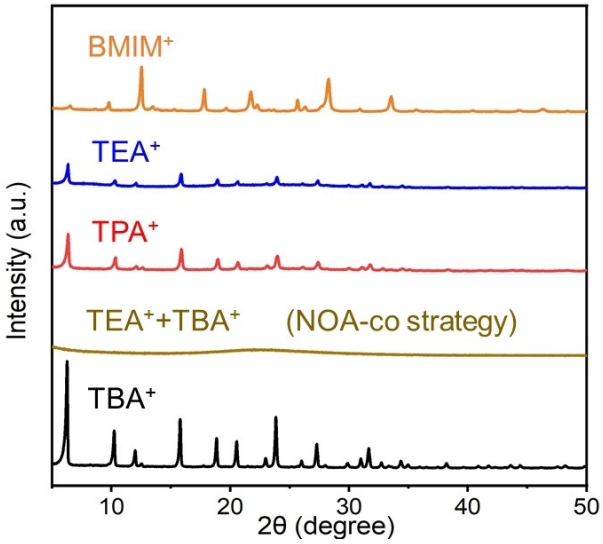

Figure 3. Product phases synthesized with different OSDAs at 160 °C for 6 h.

crystallinity of the solids increases continuously in 16 h. The solid yield and SAR at 0 h are 43.3 % and 19.4 respectively. Both of them show a minimum at 3 h, and then rise almost simultaneously until the end of the crystallization. Table S4 lists the SAR variations of liquid-phase species during the crystallization course. The high values imply that Al species mainly exist in solid phase, and the dissolution of Si source causes the decrease of solid yields before 3 h. Subsequently, the gradually increased solid yields and SAR suggest the involvement of liquid-phase Si-rich species. Given that EDS analyses (Figure S9) reveal that the amorphous particles of 3 h, 6 h, 8 h and 11 h samples possess less changed SAR of 11–12, it is speculated that the liquid-phase Si-rich species should directly participant in the formation of high-silica FSY crystals. This is further supported by the homogeneous composition distribution in the crystals of the 16 h sample (15.7 by XPS vs 16.0 by XRF). In addition, the Na/Al ratio of the solids displays a dropping trend with time, while the content of TBAOH rises gradually, which are in line with the evolution of solid crystallinity.

The SEM images of the samples are shown in Figure 4c. It can be found that the seeds in the 0 h sample have been dissolved/fragmentized (Figure S10), which agrees with the weak XRD intensity of the sample. EDS analysis indicates that the etched $USY_{38.4}$ seeds have a reduced SAR of 12.7 (Figure S11), which is comparable with the alkali-etched one (Table S3). Small crystals can be clearly discerned on the external surface of amorphous particles in the 3 h sample. Following the proceeding of crystallization, these crystals grow at the expense of amorphous materials, and the inhomogeneity in crystal sizes becomes obvious. After 16 h, amorphous precursors are completely consumed, consistent with the highest crystallinity of this product.

Based on the above results, the growth pathway of FSY-$16h_{16.0}$ zeolite is proposed as follows (Figure 4d). Both silica source and USY seeds suffer a dissolution at the initial

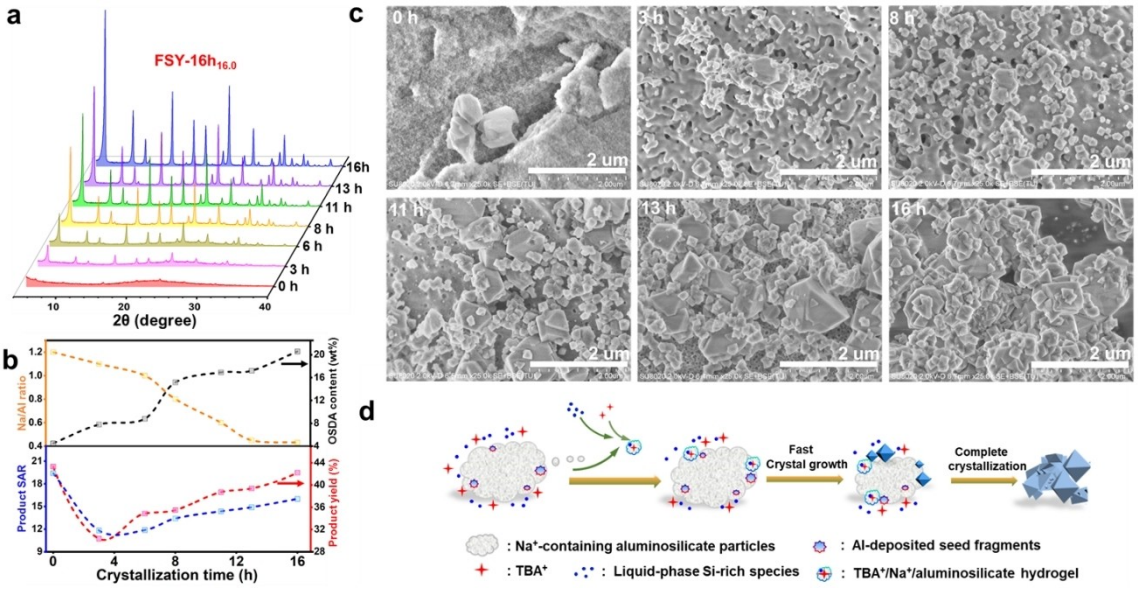

Figure 4. The evolution of a) XRD pattern, b) OSDA content (black), Na/Al ratio (yellow), SAR (blue) and yield (red) and c) morphology of the solid products during the crystallization process of FSY-16h$_{16.0}$. d) The proposed crystallization mechanism of FSY-16h$_{16.0}$.

stage. Meanwhile, the Al species deposit on the seeds and silica source, providing protection effect to avoid their excessive dissolution. The formed Al-stabilizing seed fragments possess large S_{exter}/V_{meso} and powerful induction activity. Subsequently, Na^+-containing aluminosilicate precursors at the outer surface of solid particles rearrange under the participance of liquid-phase Si species and TBA^+ and then form hydrogel with SAR of ≈16. The hydrogel microparticles migrate to the surface of seeds, wherein surface-induced nucleation works, leading to the growth of crystals with homogeneous composition distribution. As the crystallization process occurs at elevated temperature, it is completed in a very short duration.

It is well-known that scale-up synthesis is important, but sometimes challenging exercise for zeolite production, which may limit the practical application of zeolites. Herein, the scale-up synthesis of FSY-16h$_{16.0}$ was carried out by using a 10 L Parr auloclave to verify the practicability of our synthesis strategy. As shown in Figure 5, the XRD pattern and SEM image confirm the good crystallinity and purity of the scale-up product (named FSY-16h$_{16.0}$-S). The solid yield and SAR are 42.0 % and 15.9 respectively, comparable to the results of 50 mL autoclave. This result demonstrates that the strategy developed in this work is applicable for large scale production. Moreover, in attempting to improve the utilization of synthesis sources, the mother liquid after the synthesis was collected and reused for new batch of synthesis. As shown in Figure S12, the mother liquid was clear solution with particle sizes of 20–30 nm measured by dynamic light scattering. Given that no residual Al was detected and liquid ^{13}C NMR spectrum evidenced the intactness of TBAOH in mother liquid, only Al source and seeds were added in the liquid, which followed by heating at 160 °C for 8 hours. After crystallization, zeolite Y (named R-FSY-8h$_{10.3}$) was obtained with solid yield of 24.7 % and SAR

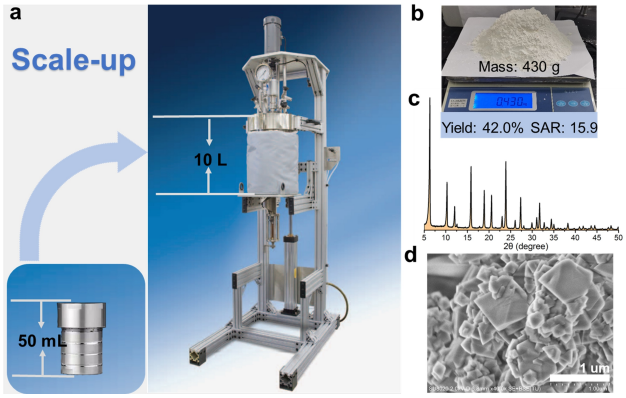

Figure 5. The scale-up synthesis of FSY-16h$_{16.0}$. a) Photos of 50 mL and 10 L Parr authoclaves. b) Product powder, c) XRD pattern and d) SEM image of solid product. The effective volume of the 10 L autoclave is 8.8 L. The $V_{gel}/V_{autoclave}$ is ≈60 % for the scale-up synthesis.

of 10.3. This preliminary result implies that the mother liquid can be reused for the fast synthesis of FSY.

The ammonia temperature-programmed desorption (NH_3-TPD) was used to investigate the acidity of the H-form FSY zeolites. Meanwhile, two commercial USY were employed as reference samples (HUSY$_{10.6}$ and HUSY$_{13.7}$, Table S1). As displayed in Figure S13, HFSY-5h$_{11.8}$, and HFSY-5h$_{13.8}$ possess comparable moderate/strong acid amounts, which suggests a decreased framework dealumination degree following the increase of zeolite SAR. HFSY-16h$_{16.0}$-S and HFSY-16h$_{18.2}$ show decreased acid amount as compared to the above two HFSY samples, likely owing to its high SAR. Interestingly, all the HFSY samples possess larger amount of moderate/strong acid sites than HUSY. As the XPS analysis (Table S5) revealed that there exists obvious dealumination gradient in USY crystals, it is

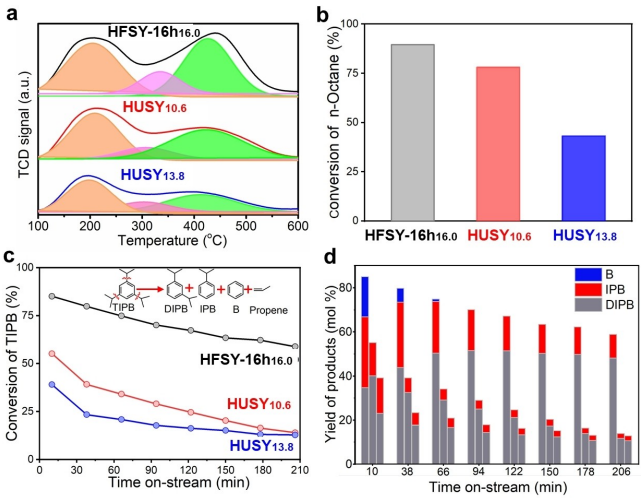

Figure 6. The comparison of acidity and catalytic cracking activity of HFSY-16h$_{16.0}$-S and HUSY zeolites. a) NH_3-TPD profiles; b) initial conversion of *n*-octane, $T=500\,°C$, $WHSV_{n\text{-octane}}=12.6\ h^{-1}$, TOS = 5 min; c) TIPB cracking versus time on stream, $T=160\,°C$, $WHSV_{TIPB}=3.2\ h^{-1}$; d) product yields of TIPB cracking (HFSY-16h$_{16.0}$-S, left; HUSY$_{10.6}$, middle; HUSY$_{13.8}$, right). B, IPB and DIPB represent benzene, cumene and diisopropylbenzene isomers, respectively.

speculated that the Al atoms in the Al-rich region are easier to be dealuminated and cause the reduced acid amounts of USY. Besides, surface Si or Al deposition on USY samples may reduce the concentration of acid sites on the crystal shell. Pyridine adsorbed FTIR spectra were further recorded to learn the accessibility of acid sites. From Figure S14, both the acidic hydroxyls in the supercages and SOD cages show a clear decrease after pyridine desorption at 150 °C for the investigated samples, implying that the Brønsted acid sites (BAS) in the SOD cages can transfer to supercages under the induction of alkaline molecules.[20] The relatively large amount of inaccessible BAS in the SOD cages of USY$_{10.6}$ may be due to its serious dealumination gradient, leaving a low silica core with much crowded acid sites.

The catalytic activities of the samples were evaluated in the cracking reactions of *n*-octane and 1,3,5-triisopropylbenzene (1,3,5-TIPB). The scale-up HFSY-16h$_{16.0}$-S, possessing both higher solid yield and considerable amount of acid sites, was employed for the investigation. From Figure 6, HFSY-16h$_{16.0}$-S exhibits higher *n*-octane conversion than two HUSY samples. The activity sequence of the samples is in positive correlation with their acid amount. For 1,3,5-TIPB cracking, HFSY-16h$_{16.0}$-S also displays superior cracking activity, which should result from its homogeneous acid distribution and larger acid amount. The yields of deep cracking products on HFSY-16h$_{16.0}$-S are also higher than on HUSY. These results demonstrate the remarkably catalytic cracking performance of HFSY zeolite.

Conclusion

The novel strategy developed in this work opens the door to the synthesis of zeolite Y with both highly siliceous framework and fast crystallization rate under mild conditions and with commercial reagents. It has been demonstrated the use of TBAOH is essential for the control of phase purity at elevated temperature owing to the strong interactions of TBA^+ with the FAU framework. Moreover, the induction activity of USY zeolites strongly depends on the nature of their etched fragments in the initial alkaline gel; higher SAR and large S_{exter}/V_{meso} are key parameters for them to inducing fast crystal growth. Under the cooperation of high crystallization temperature, TBAOH and USY seeds, high-silica zeolite Y can be obtained in 5–16 h at 160 °C. The synthesis strategy is further demonstrated to be applicable for large scale production. The resulting FSY materials possess high (hydro)thermal stability and plentiful strong acid sites, which make them an extraordinary solid acid catalyst, especially for converting bulky reactants. It is envisioned that this strategy will benefit the efficient synthesis of zeolitic materials and the applications of high-silica zeolite Y.

Acknowledgements

This work is supported by the National Natural Science Foundation of China (21991090, 21991091), the Key Research Program of Frontier Sciences, CAS (QYZDB-SSW-JSC040, QYZDY-SSW-JSC024) and DICP Funding (DICP ZZBS201807).

Conflict of Interest

The authors declare no conflict of interest.

Data Availability Statement

The data that support the findings of this study are available in the Supporting Information of this article.

Keywords: Catalytic Cracking · Fast Synthesis · High-Silica Y · Zeolites

[1] a) C. Martínez, A. Corma, *Coord. Chem. Rev.* **2011**, *255*, 1558–1580; b) J. Shi, Y. Wang, W. Yang, Y. Tang, Z. Xie, *Chem. Soc. Rev.* **2015**, *44*, 8877–8903.

[2] a) D. Verboekend, N. Nuttens, R. Locus, J. Van Aelst, P. Verolme, J. C. Groen, J. Perez-Ramirez, B. F. Sels, *Chem. Soc. Rev.* **2016**, *45*, 3331–3352; b) N. Eng-Poh, D. Chateigner, T. Bein, V. Valtchev, S. Mintova, *Science* **2012**, *335*, 70–73; c) P. Bai, U. J. Etim, Z. F. Yan, S. Mintova, Z. D. Zhang, Z. Y. Zhong, X. H. Gao, *Catal. Rev. Sci. Eng.* **2019**, *61*, 333–405; d) J. García-Martínez, K. Li, G. Krishnaiah, *Chem. Commun.* **2012**, *48*, 11841–11843.

[3] a) M. Shahinuzzaman, Z. Yaakob, Y. Ahmed, *Renewable Sustainable Energy Rev.* **2017**, *77*, 1375–1384; b) G. J. Gomes, D. M. Dal Pozzo, M. Fernanda Zalazar, M. B. Costa, P. A. Arroyo, P. R. S. Bittencourt, *Top. Catal.* **2019**, *62*, 874–883; c) T. Ennaert, J. Van Aelst, J. Dijkmans, R. De Clercq, W. Schutyser, M. Dusselier, D. Verboekend, B. F. Sels, *Chem. Soc. Rev.* **2016**, *45*, 584–611; d) T. T. Yan, S. K. Yao, W. L. Dai, G. J. Wu, N. J. Guan, L. D. Li, *Chin. J. Catal.* **2021**, *42*, 595–605.

[4] a) W. Vermeiren, J.-P. Gilson, *Top. Catal.* **2009**, *52*, 1131–1161; b) C. Martínez, D. Verboekend, J. Pérez-Ramírez, A. Corma, *Catal. Sci. Technol.* **2013**, *3*, 972–981; c) U. J. Etim, B. J. Xu, Z. Zhang, Z. Y. Zhong, P. Bai, K. Qiao, Z. F. Yan, *Fuel* **2016**, *178*, 243–252; d) C. Schroeder, M. R. Hansen, H. Koller, *Angew. Chem. Int. Ed.* **2018**, *57*, 14281–14285; *Angew. Chem.* **2018**, *130*, 14477–14481.

[5] a) G. Agostini, C. Lamberti, L. Palin, M. Milanesio, N. Danilina, B. Xu, M. Janousch, J. A. van Bokhoven, *J. Am. Chem. Soc.* **2010**, *132*, 667–678; b) W. Lutz, *Adv. Mater. Sci. Eng.* **2014**, 724248.

[6] a) M. C. Silaghi, C. Chizallet, P. Raybaud, *Microporous Mesoporous Mater.* **2014**, *191*, 82–96; b) M. C. Silaghi, C. Chizallet, J. Sauer, P. Raybaud, *J. Catal.* **2016**, *339*, 242–255.

[7] J. Wang, P. Liu, M. Boronat, P. Ferri, Z. Xu, P. Liu, B. Shen, Z. Wang, J. Yu, *Angew. Chem. Int. Ed.* **2020**, *59*, 17225–17228; *Angew. Chem.* **2020**, *132*, 17378–17381.

[8] M. Moliner, F. Rey, A. Corma, *Angew. Chem. Int. Ed.* **2013**, *52*, 13880–13889; *Angew. Chem.* **2013**, *125*, 14124–14134.

[9] F. Delprato, L. Delmotte, J. L. Guth, L. Huve, *Zeolites.* **1990**, *10*, 546–552.

[10] D. L. Zhu, L. Y. Wang, D. Fan, N. N. Yan, S. J. Huang, S. T. Xu, P. Guo, M. Yang, J. M. Zhang, P. Tian, Z. M. Liu, *Adv. Mater.* **2020**, *32*, 2000272.

[11] Q. Ke, I. Khalil, B. Smeyers, Z. Li, R. Oliveira-Silva, B. Sels, D. Sakellariou, M. Dusselier, *Angew. Chem. Int. Ed.* **2021**, *60*, 24189–24197; *Angew. Chem.* **2021**, *133*, 24391–24399.

[12] a) D. W. He, D. h. Yuan, Z. J. Song, Y. S. Tong, Y. Q. Wu, S. T. Xu, Y. P. Xu, Z. M. Liu, *Chem. Commun.* **2016**, *52*, 12765–12768; b) M. Borel, M. Dodin, T. J. Daou, N. Bats, B. Harbuzaru, J. Patarin, *Cryst. Growth Des.* **2017**, *17*, 1173–1179.

[13] H. Kacirek, H. Lechert, *J. Phys. Chem.* **1976**, *80*, 1291–1296.

[14] a) Z. Liu, T. Wakihara, K. Oshima, D. Nishioka, Y. Hotta, S. P. Elangovan, Y. Yanaba, T. Yoshikawa, W. Chaikittisilp, T. Matsuo, T. Takewaki, T. Okubo, *Angew. Chem. Int. Ed.* **2015**, *54*, 5683–5687; *Angew. Chem.* **2015**, *127*, 5775–5779; b) Z. Liu, T. Wakihara, N. Nomura, T. Matsuo, C. Anand, S. P. Elangovan, Y. Yanaba, T. Yoshikawa, T. Okubo, *Chem. Mater.* **2016**, *28*, 4840–4847.

[15] a) L. Zhu, L. Ren, S. Zeng, C. Yang, H. Zhang, X. Meng, M. Rigutto, A. Made, F. S. Xiao, *Chem. Commun.* **2013**, *49*, 10495–10497; b) J. Wang, L. Y. Wang, D. L. Zhu, W. h. Cui, Y. F. Wang, T. Peng, Z. M. Liu, *Chem. J. Chin. Univ.* **2021**, *42*, 1–10; c) S. Ferdov, K. Tsuchiya, N. Tsunoji, T. Sano, *Microporous Mesoporous Mater.* **2019**, *276*, 154–159.

[16] M. Maldonado, M. D. Oleksiak, S. Chinta, J. D. Rimer, *J. Am. Chem. Soc.* **2013**, *135*, 2641–2652.

[17] J. Anwar, S. Khan, L. Lindfors, *Angew. Chem. Int. Ed.* **2015**, *54*, 14681–14684; *Angew. Chem.* **2015**, *127*, 14894–14897.

[18] a) C. S. Cundy, P. A. Cox, *Chem. Rev.* **2003**, *103*, 663–701; b) J. Y. Li, A. Corma, J. h. Yu, *Chem. Soc. Rev.* **2015**, *44*, 7112–7127; c) M. D. Oleksiak, K. Muraoka, M. F. Hsieh, M. T. Conato, A. Shimojima, T. Okubo, W. Chaikittisilp, J. D. Rimer, *Angew. Chem. Int. Ed.* **2017**, *56*, 13366–13371; *Angew. Chem.* **2017**, *129*, 13551–13556.

[19] D. Yuan, D. He, S. Xu, Z. Song, M. Zhang, Y. Wei, Y. He, S. Xu, Z. Liu, Y. Xu, *Microporous Mesoporous Mater.* **2015**, *204*, 1–7.

[20] L. Lakiss, C. Kouvatas, J. P. Gilson, H. A. Aleksandrov, G. N. Vayssilov, N. Nesterenko, S. Mintova, V. Valtchev, *Angew. Chem. Int. Ed.* **2021**, *60*, 26702–26709; *Angew. Chem.* **2021**, *133*, 26906–26913.

Manuscript received: December 27, 2021
Accepted manuscript online: March 22, 2022
Version of record online: April 5, 2022